https://ntrs.nasa.gov/search.jsp?R=19750023445 2020-03-19T21:27:03+00:00Z

COMPARISON OF NASTRAN AND MITAS NONLINEAR THERMAL ANALYSES OF A CONVECTIVELY COOLED STRUCTURE*

Earl A. Thornton
Old Dominion University

and

Allan R. Wieting
NASA Langley Research Center

33

ABSTRACT

Comparative steady-state nonlinear thermal analyses of a scramjet fuel injection strut are presented. The analyses were performed using the NASTRAN finite-element program and MITAS, a lumped-parameter thermal analyzer. The strut is subjected to aerodynamic heating on two sides and is internally cooled by hydrogen flowing from internal manifolds through heat exchangers bonded to the primary structure. Based on coolant temperatures determined by MITAS, NASTRAN predicted temperature distributions throughout the strut which were in close agreement with similar MITAS predictions.

INTRODUCTION

A research program is under way at the Langley Research Center to develop an airframe-integrated hydrogen-fueled scramjet (supersonic combustion ramjet) concept designed to operate over a flight Mach number range from 4 to 10. This concept (See fig. 1) utilizes the entire undersurface of the aircraft to process the engine air flow. The aircraft forebody serves as an extension of the engine inlet and the afterbody serves as an extension of the engine nozzle. Hydrogen fueled scramjets are of interest because no other airbreathing engine can match the efficiency of the scramjet above Mach 6 and hydrogen offers high energy content and cooling capacity along with minimal environmental impact. The high cooling capacity of the hydrogen can be used to cool the engine surfaces prior to combustion and thereby accommodate the extremely hostile environment which exists within scramjets.

---

*The NASTRAN analysis portion of this study was carried out by the first author at the Langley Research Center under support of NASA grant number NSG 1093 to the Old Dominion University Research Foundation.

A preliminary thermal/structural design and analysis study of the engine has been previously performed to determine design feasibility, coolant requirements, and structural mass estimates (ref. 1). Results of the study indicated that the fuel injection struts presented the most formidable cooling and structural problems. A more detailed study of the fuel injection struts is currently under way to further define cooling requirements and thermal/structural behavior. A thermal analyzer based on a finite element formulation is available in NASTRAN to provide thermal/structural analysis. However, there is little user experience with the NASTRAN thermal analyzer in the analysis of convectively cooled structures. Consequently, as part of the strut study, an evaluation of the NASTRAN thermal analyzer capabilities related to convectively cooled structures was undertaken. This evaluation is achieved through a comparison of results with an established finite-difference lumped-parameter thermal analyzer, MITAS (Martin Interactive Thermal Analysis System, ref. 2). The purpose of this paper is to present the results of this comparative evaluation.

SYMBOLS

h Convective heat transfer coefficient, W/m^2-K (BTU/ft^2-s-°R)

h_o Reference convective heat transfer coefficient, W/m^2-K (BTU/ft^2-s-°R)

k Thermal conductivity, W/m-K (BTU/ft-s-°R)

k_o Reference thermal conductivity, W/m-K (BTU/ft-s-°R)

ℓ Strut thickness, 2.74 cm (1.08 in.)

L Strut chord length, 30.7 cm (12.1 in.)

$\dot{q}$ Aerodynamic heating rate, W/m^2 (BTU/ft^2-s)

T Temperature, K (°R)

x,y Distances along X- and Y-axes, respectively (origin at virtual apex)

FUEL INJECTION STRUTS

The three fuel injection struts (See fig. 1) resemble highly swept airfoils. The side struts are considered in the present study because their unsymmetrical configuration and loading lead to complex thermal/structural behavior. A chordwise cross section of a side strut is shown in figure 2. The side struts have a maximum thickness of 2.74 cm (1.08 in.), chord length of 30.7 cm (12.1 in.), a span of 45.7 cm (18 in.) and are swept back 48°. Each strut is subdivided internally into four chordwise compartments: the fore-and-aft compartments are coolant inlet and outlet

manifolds, respectively, and the central compartments are fuel manifolds for the strut trailing edge and wall fuel injectors. (Fuel injector details are not shown; see ref. 1). Heat shields are installed in all but the forward compartment, as shown, to eliminate direct convective heating from the hydrogen to the primary structure.

Coolant at 55 K (100°R) in the forward manifold is injected through a slot, impinges on the leading edge, and splits (unequally) to flow through an offset-fin plate-fin heat exchanger (See fig. 3) which is brazed to the primary structure. Flow proceeds along each wall to the trailing edge where it is collected in the aft manifold at approximately 890 K (1600°R).

The struts are subjected to severe temperature gradients because of nonuniform aerodynamic heating and variations in hydrogen temperatures in the manifolds. As shown in figure 4, the aerodynamic heating is different for each side wall and varies considerably along either wall because of flow stagnation at the leading edge, boundary-layer—shock interactions, and combustion. The thermal conductivities of the structure and the convective heat-transfer coefficient vary significantly with temperature as shown in figure 5, and thus a nonlinear steady-state thermal analysis is required to accurately predict strut temperatures. The strut is also subjected internally to high hydrogen pressures and must withstand a large unbalanced side loading resulting from possible unsymmetrical engine unstart.

NASTRAN ANALYSIS

A two-dimensional finite-element model of a typical chordwise cross section was formulated by using a total of 4657 elements. The discretization was made primarily to give an accurate temperature distribution throughout the strut, but an additional objective was to permit the same finite-element model to be used for both the thermal analysis and a subsequent plane strain structural analysis. It was desirable to use essentially the same models since the complex section and loadings required fine detail to predict temperature and stress distributions throughout the strut cross section.

The finite-element representation of conduction and convection heat transfer at a typical wall section is shown in figure 6. The NASTRAN CQDMEM element was used to represent the conduction heat transfer in the primary structure and the aerodynamic skin since this is the only NASTRAN quadrilateral element which has heat-transfer capability. Four membrane elements were used through the thickness of the primary structure because it was known from the preliminary study (ref. 1) that temperature gradients and wall bending stresses were significant. Since a nonuniform thermal gradient occurs across the coolant passage, conduction through the heat exchanger fins was represented by four rod elements in series. A total of 255 sets of four rod elements was used to represent the conduction through the heat exchanger fins for the strut cross section.

Line convection elements (shown in fig. 6 as dashed lines) were used to represent the convective heat transfer between the hydrogen in the manifolds and the primary structure and between the hydrogen and the wetted surfaces in the coolant passages. Convection elements were also used to represent the aerodynamic heating on the external skin.

A basic difficulty in the NASTRAN thermal analysis arose in modeling the convective heat transfer due to flow of the hydrogen coolant. NASTRAN has no direct means for modeling heat transfer due to fluid flow. Thus it was not possible by using NASTRAN to determine the coolant temperature distribution along the passage. Instead it was necessary to compute the coolant bulk temperatures by using the finite-difference thermal analyzer MITAS (ref. 2). These data were supplied to NASTRAN as a boundary condition using the convective line element.

Significant characteristics of the NASTRAN thermal finite-element model are shown in table I. The model is characterized by a large number of nodes and elements. The data cards for the model were generated by special purpose FORTRAN programs. The node and convection data were checked prior to execution by generating undeformed NASTRAN structural plots. Since NASTRAN does not have the capability to plot convection line elements, duplicate dummy plotting elements (PLOTEL) were generated to represent convection elements. Most of the convection data were checked this way; however, it would be desirable to have a direct means of plotting the convection line elements.

TABLE I. CHARACTERISTICS OF NASTRAN FINITE-ELEMENT THERMAL MODEL

Item	Number
Nodes	
Known Temperatures	595
Unknown Temperatures	2812
Total	3407
Conductors	
Conduction	
Membrane elements	1517
Rod elements	1026
Convection	
Surface elements	2114
Total	4657

Before NASTRAN execution, the nodes were resequenced by using a FORTRAN program based upon the renumbering algorithm developed in reference 3. The NASTRAN conduction matrix of size 2812 had a semi-bandwidth of 278 for the original numbering scheme. The semi-bandwidth was reduced to 34 by renumbering of the nodes. The NASTRAN resequencing cards were generated by the renumbering program. The basic NASTRAN data deck which consisted of about 15000 cards was stored on a problem tape and executed by using the NASTRAN restart capability.

Two NASTRAN thermal analyses were performed. First, a linear analysis was made with constant values for the thermal conductivities and convection coefficients. Then, the resulting temperature distribution was used as the initial estimate for the iterative nonlinear NASTRAN thermal analysis.

MITAS ANALYSIS

The finite-difference thermal analyzer MITAS is used as the basis for the comparative evaluation. MITAS uses an equivalent lumped-parameter electrical-circuit analogue of the thermal system. In this technique the physical structure is divided into subvolumes which are assumed to be at a temperature corresponding to their center. The physical system is replaced by a network of conductors between the centers, or nodal points, of the subvolumes. The conductor may represent conduction, convection, or radiation heat flow paths. The electrical analogue of the thermal model for a typical section of the strut is given in figure 7.

Although a coarser model for MITAS may have been adequate, a one to one correspondence between the MITAS nodes and the NASTRAN grid points was established to eliminate discrepancies due to differences in discretization. Significant characteristics of the MITAS finite difference thermal model are given in table II. There were 3106 unknown temperatures in the MITAS analysis compared with 2812 unknown temperatures in the NASTRAN analysis. The additional MITAS unknowns are essentially the unknown coolant temperatures.

Data preparation for MITAS consisted of assigning node numbers, conductor numbers, and conductance values. With the MITAS internal generation capability, 98 percent, 82 percent, and 71 percent of the nodes, conductors, and conductances, respectively, were automatically generated. This represents an overall automated generation of 68 percent of the required input data. Spatial coordinates are not input to the MITAS model; consequently, plots of the finite-difference model could not be obtained for an input data check. The MITAS deck consisted of 3200 cards. MITAS, programmed as a preprocessor, reads the input data and incorporates it into a source program to obtain the required solution. This program was stored on a tape to yield a restart capability at any point within the solution sequence.

TABLE II. CHARACTERISTICS OF MITAS THERMAL MODEL

Item	Number
Nodes	
Known Temperatures	283
Unknown Temperatures	3106
Total	3389
Conductors	
Conduction	4443
Convection	
Surface	1862
Fluid	290
Total	6595

RESULTS AND DISCUSSIONS

Comparative NASTRAN and MITAS predicted temperature distributions within the strut cross section are presented in figures 8 to 11.

Of particular interest are the temperatures in the hydrogen coolant and the temperatures along the aerodynamic skin. Accurate prediction of the temperature distribution along the aerodynamic skin is required to predict the fatigue life of the heat exchanger. Plots of these temperature distributions are shown for the starboard side of the strut in figure 8. The temperature distribution in the hydrogen coolant was predicted by MITAS and used as input to NASTRAN.

The aerodynamic skin temperature distribution (fig. 8) basically reflects the aerodynamic heating distribution shown in figure 4. The skin temperature is high at the leading edge because of stagnation heating, drops sharply with a drop in the aerodynamic heating and maintains a nearly uniform value up to about $x/L = 0.5$, after which the temperature increases rapidly with rising aerodynamic heating first due to shock-boundary layer interaction and then combustion. The sharp rise of the skin temperature at $x/L = 0.59$ and at the trailing edge are local effects due to an absence of heat exchanger fins which result in a reduction of heat transfer to the hydrogen coolant. Heat exchanger fins were omitted in these regions because of possible fabrication problems.

The agreement between NASTRAN and MITAS predictions for this temperature distribution is very good. Some of the temperature values predicted by the two programs shown in figure 8 are tabulated in table III.

TABLE III. COMPARATIVE TEMPERATURE VALUES ALONG STARBOARD AERODYNAMIC SKIN

	Temperature (K)		
x/L	NASTRAN	MITAS	% Difference
0.05	955	951	0.4
0.1	137	139	1.4
0.2	142	143	0.6
0.3	148	148	0
0.4	154	154	0
0.5	165	165	0
0.6	307	318	3.5
0.7	463	465	0.4
0.8	639	650	1.7
0.9	759	770	1.5
1.0	881	887	0.7
1.05	1060	1120	5.7

The tabulated values indicate that agreement of temperatures predicted at the stagnation point is excellent and that the largest difference in the predicted temperatures, about 6 percent, occurs on the trailing edge. Similar results, which are not shown, were obtained for the port-side aerodynamic skin.

Of additional interest are the temperature gradients in the primary structure. In the previous study (ref. 1) these gradient were shown to introduce critical levels of thermal stresses. Temperature distributions in the starboard primary structure as predicted by NASTRAN and MITAS are shown in figure 9. Predictions for the structural temperatures along the hydrogen coolant passage and along the manifolds are shown. The temperatures in the primary structure reflect the hydrogen coolant temperature distribution and the heat transfer from the hydrogen in the

internal manifolds. On the coolant side of the primary structure, the structural temperatures basically follow the coolant temperature distribution shown in figure 8. On the manifold side the large increase in temperature of the structure at x/L = 0.5 is due to convective heating from the 890 K (1600°R) hydrogen in the adjacent manifold.

The agreement between the predicted temperatures is excellent. The programs calculate almost identical thermal gradients through the primary structure including the important reversal in sign of the gradient which occurs across the center bulkhead at about x/L = 0.5. The programs also show good agreement in calculating local effects such as the local peaks and valleys in the temperatures along the manifold side of the strut at the points of attachment to the thin interior bulkheads, e.g. at x/L = 0.3, and the rapid rise in temperature at x/L = 0.5.

Variations of the temperature through the thickness of the strut cross section are shown in figures 10 and 11 at the forward and aft main interior bulkheads. These plots show values of temperature at nodes on the aerodynamic skin, the heat exchanger fins, and on the primary structure. Figure 10 shows the temperature distribution through the center of the forward bulkhead. It can be seen that the temperature in the bulkhead at $y/\ell = 0.5$ approaches the temperature of the hydrogen in the adjacent manifold, about 55 K (100°R). NASTRAN and MITAS predictions show excellent agreement for all values of y. Figure 11 presents temperature distributions at the aft bulkhead for both the bulkhead and adjacent heat shield. The figure shows the effect of the heat shield on the temperatures in the bulkhead and walls of the primary structure. Although the bulkhead is heated close to the temperature of the hydrogen in the adjacent manifolds (890 K, 1600°R), the heat shield causes a substantial drop in the temperatures of the walls of the primary structure at $y/\ell = 0.15$ and $y/\ell = 0.75$. Values for the temperatures at x/L = 0.686 plotted in figure 11 are tabulated in table IV.

The most significant difference in predicted temperature occurs on the heat shield at the corners. The MITAS model predicts temperatures about 14 percent higher than the NASTRAN model at these points. This discrepancy appears to be attributable to differences in the NASTRAN and MITAS models of interior corners of the heat shield. Elsewhere, table IV shows that there is very good agreement between the two solutions.

A comparison of computer storage and run times for the NASTRAN and MITAS nonlinear thermal analyses is presented in table V. Both programs were executed on the Langley Research Center CDC 6600 computer. NASTRAN was executed in a larger field length and required less CPU time but more operating system calls than MITAS. By using the LRC cost algorithm, these two analyses cost about the same amount. It should be noted, however, that a prior additional NASTRAN linear analysis was used to provide an initial temperature estimate for the NASTRAN nonlinear thermal solution. It is also noteworthy that MITAS determined temperature values for 3106 unknowns in comparison with 2812 unknowns for NASTRAN. As a further point

of importance in the cost comparison, the MITAS solution includes the generation of a significant portion of its input data. As has been noted, the NASTRAN data were prepared by using special purpose programs at additional cost. Thus, when all factors are considered for the cost of a thermal analysis only, the MITAS solution was more cost effective.

TABLE IV. COMPARATIVE TEMPERATURE VALUES ON AFT HEAT SHIELD ON REAR BULKHEAD

	Temperature, K		
y/ℓ	NASTRAN	MITAS	% Difference
0.023	261	261	0
.038	259	259	0
.063	266	264	0.7
.163	369	351	4.9
.205	696	792	13.8
.305	773	752	2.8
.405	778	770	1.0
.505	782	775	0.9
.605	776	770	0.8
.705	766	752	1.8
.784	695	792	14.0
.829	397	400	0.7
.929	314	318	1.3
.954	419	422	0.8
.969	443	444	0.2

TABLE V. COMPARISON OF NASTRAN AND MITAS NONLINEAR THERMAL ANALYSIS COMPUTER RUNS

[Langley Research Center CDC 6600]

	NASTRAN	MITAS
Field length (octal words)	220 000	167 000
Computer time (CPU seconds)	967	1 780
Operating system calls	28 000	3 300
Comparative cost (per unit cost rate)	76.7	64.9

Of further interest are the relative merits of the two programs for use in a combined thermal/structural analysis. Incompatibilities between lumped-parameter programs such as MITAS and structural analysis programs such as NASTRAN have been cited (ref. 4) as one reason for development of NASTRAN thermal analysis capability. There did not exist any incompatibility between the MITAS thermal model and a NASTRAN structural model since a one-to-one correspondence between nodes was made in the development of the MITAS model. Thus, the incompatibility problem can be avoided by proper planning in development of the thermal and structural models. Of major importance, however, is that the verified NASTRAN thermal finite-element model can be used with only slight modification for a subsequent structural analysis. If a MITAS thermal analysis alone was performed, a completely new finite-element structural model would have to be generated and verified. This fact must be considered in a final evaluation of costs for a combined thermal/structural analysis.

For the thermal analysis of convectively cooled structures, a salient fact has already been noted. MITAS possesses the capability of modeling the convective heat transfer in the fluid flow. NASTRAN, level 15.5, is limited in representing heat transfer because of fluid flow as a convective boundary condition. This restriction offsets the advantages and limits the usefulness of the NASTRAN thermal analyzer for convectively cooled structures. The inability of the NASTRAN thermal analyzer to model convective heat transfer due to fluid flow is also characteristic of some other general purpose finite-element thermal analyzers.

CONCLUDING REMARKS

Comparative two-dimensional steady-state nonlinear thermal analyses of a scramjet fuel injection strut have been performed by using NASTRAN and

MITAS. Since NASTRAN does not possess the capability to represent heat transfer due to fluid flow, a MITAS solution was obtained first. The MITAS solution provided coolant temperatures which were used as boundary conditions for the subsequent NASTRAN analysis as well as temperatures throughout the structure which were used for comparison with the NASTRAN solution.

Comparison of predicted temperature distributions along the aerodynamic skin, heat exchangers, and primary structure of the strut showed good to excellent agreement. This close agreement verifies the capability of NASTRAN to solve a large nonlinear conduction heat-transfer problem with convective boundary conditions. The good agreement also demonstrates the MITAS capability for performing a complete thermal analysis of a convectively cooled structure. A final evaluation of the accuracy of the NASTRAN solution by comparison with MITAS must await the development within NASTRAN of a means of representing convective heat transfer due to fluid flow.

A comparison of costs for the analyses showed that MITAS was slightly less expensive with an additional advantage of automated input data generation capability. An advantage of the NASTRAN program was the ability to generate structural plots for data checking purposes. A part of this advantage was nullified by an inability to plot convective boundary elements.

Since general purpose finite-element thermal analyzers cannot presently represent convective heat transfer due to fluid flow there exists a basic need for development of this capability. In light of current interest in optimization of thermal/structural designs, a means of representing convective heat transfer due to fluid flow would offer potential for optimization studies of convectively cooled structures using finite-element analysis. Until such means are developed, thermal/structural analyses of convectively cooled structures must be performed by using other methods to determine either coolant temperatures or the complete thermal solution prior to a finite-element analysis.

REFERENCES

1. Wieting, A. R.; and Guy, R. W.: Preliminary Thermal-Structural Design and Analysis of an Airframe-Integrated Hydrogen-Cooled Scramjet. Aerospace Sciences Meeting, AIAA Paper No. 75-137, January 1975.

2. Staff of Martin-Marietta Corporation: Martin Interactive Thermal Analyses System, Version 1.0. MDS-SPLPD-71-FD238 (REV3), Mar. 1972.

3. Collins, R. J.: Bandwidth Reduction by Automatic Renumbering. Internat. J. Numer. Meth. Eng., vol. 6, 1973, pp. 345-356.

4. Lee, Hwa-Ping; and Mason, James B.: NASTRAN Thermal Analyzer, A General Purpose Finite Element Heat Transfer Computer Program. NASTRAN Users' Experiences, NASA TM X-2637, 1972, pp. 443-454.

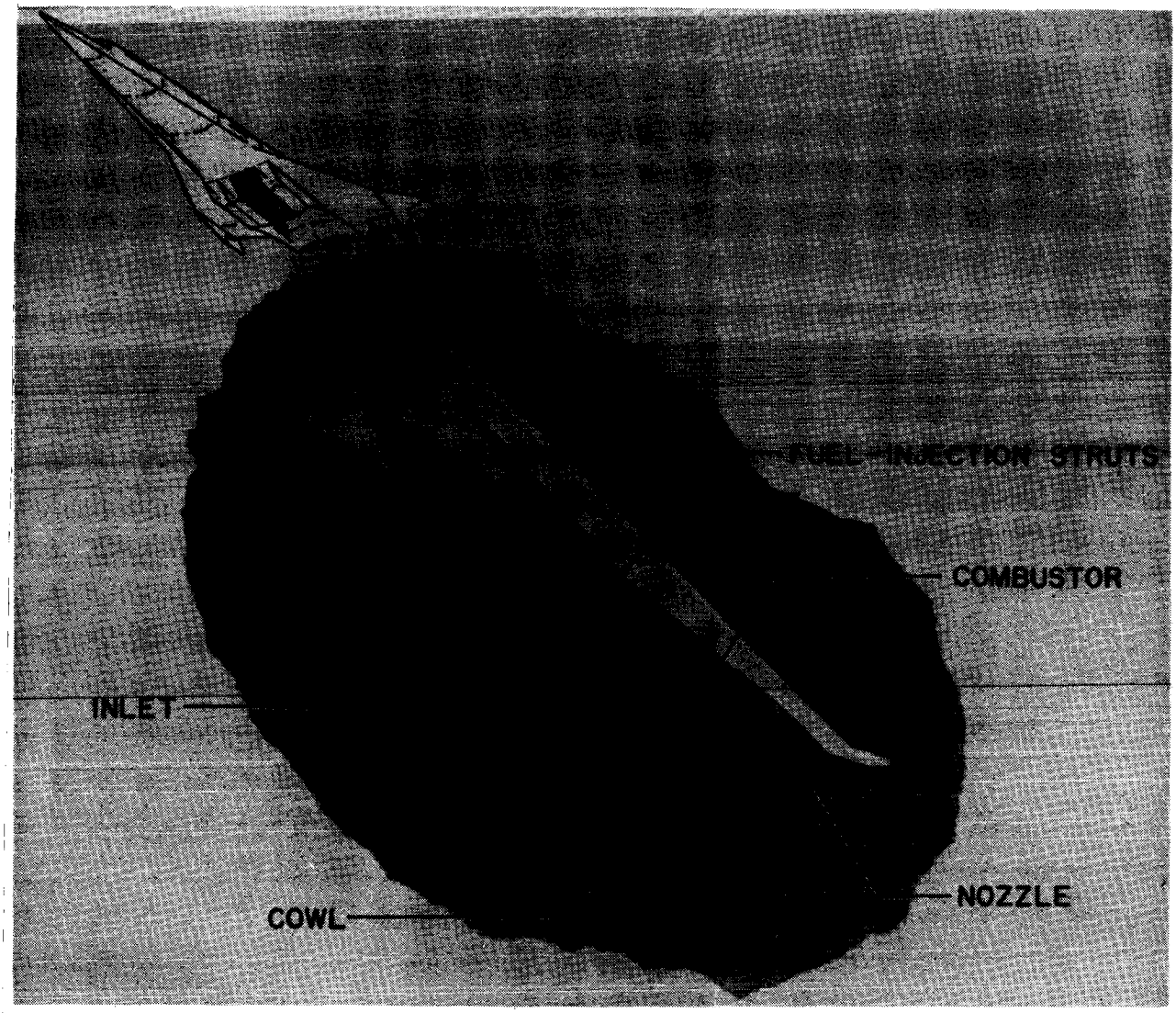

Figure 1. - Airframe-integrated scramjet concept.

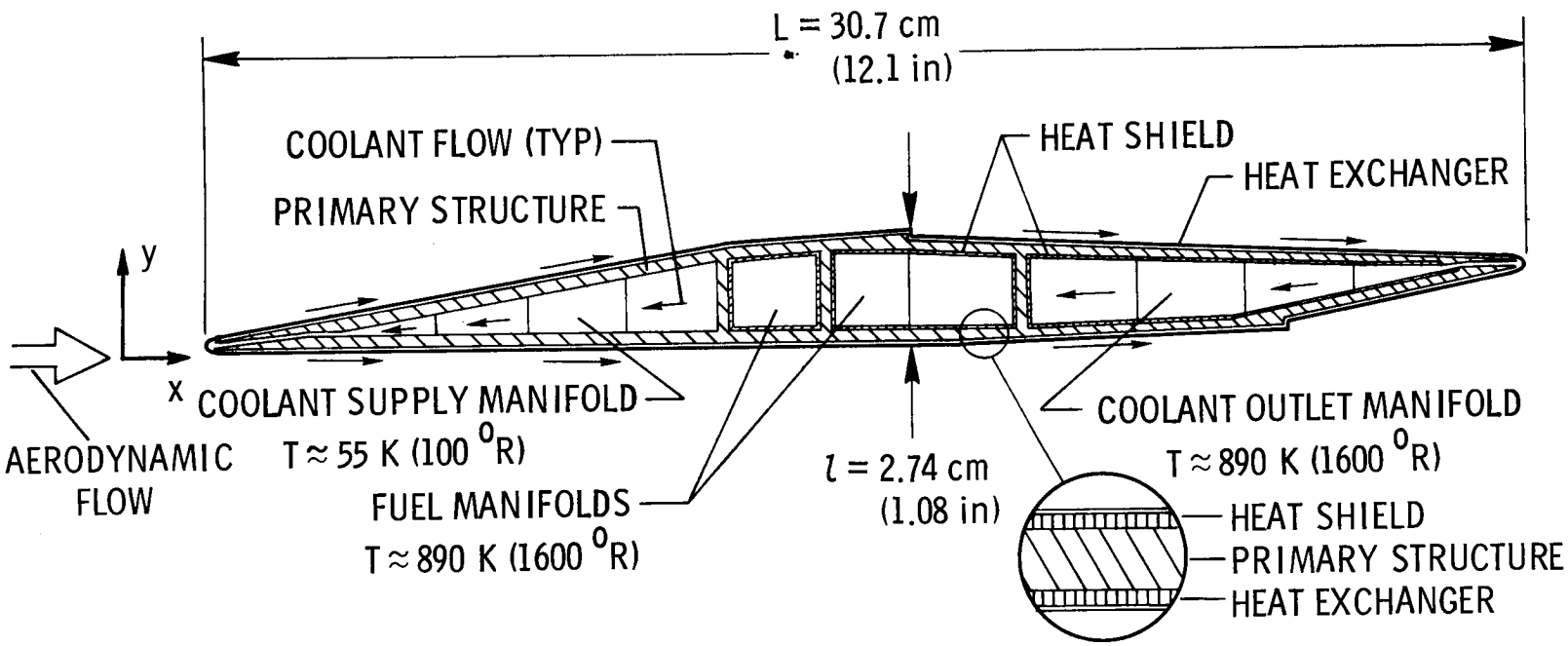

Figure 2. - Fuel-injection strut cross section (chordwise).

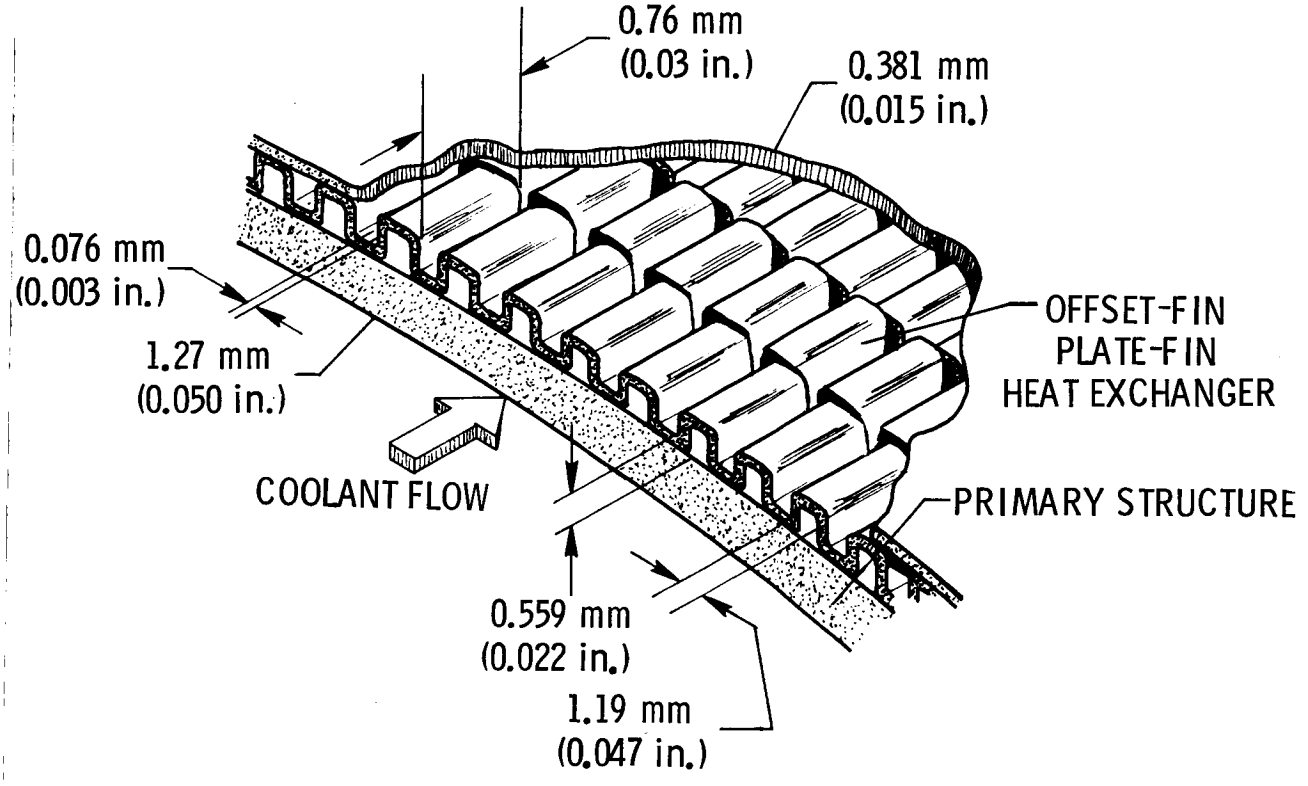

Figure 3. - Typical rectangular offset-fin plate-fin heat exchanger.

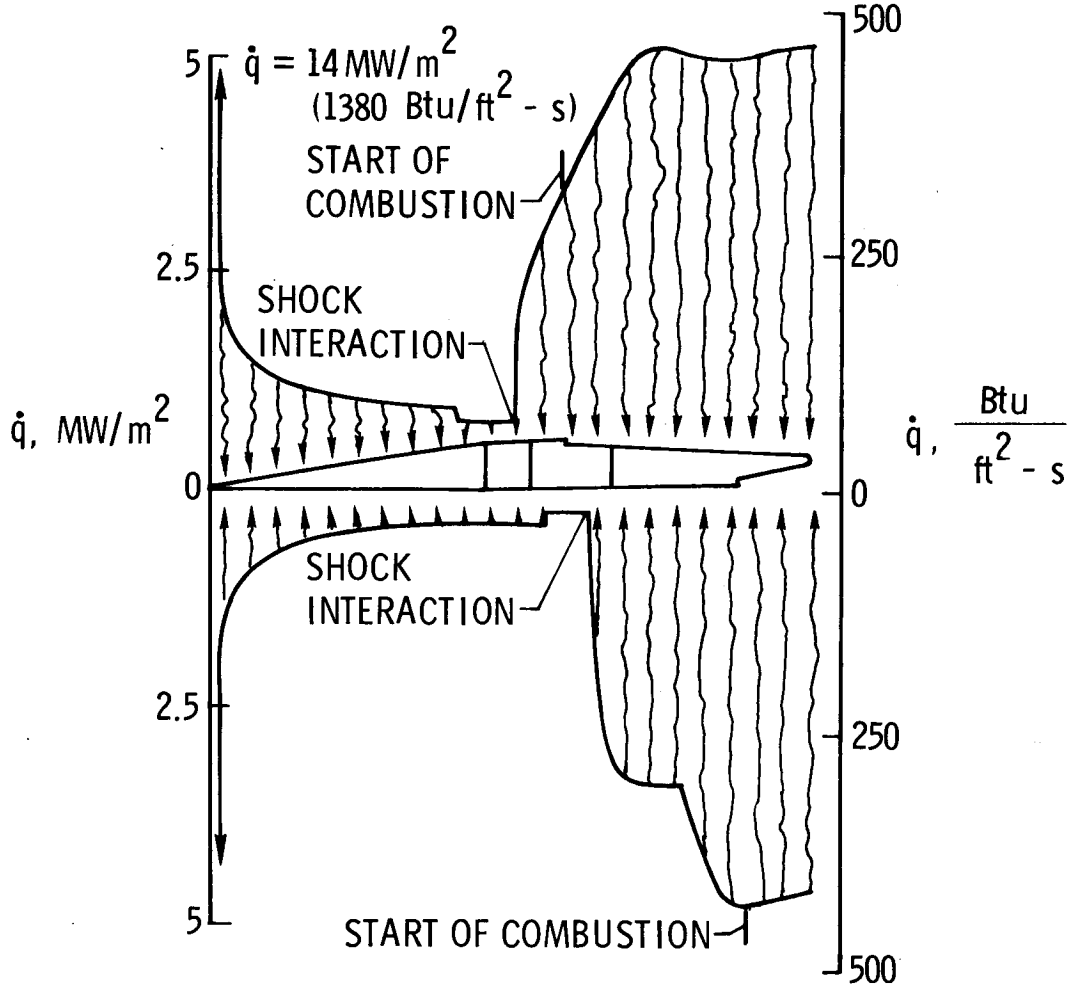

Figure 4. - Aerodynamic heating rate distributions.

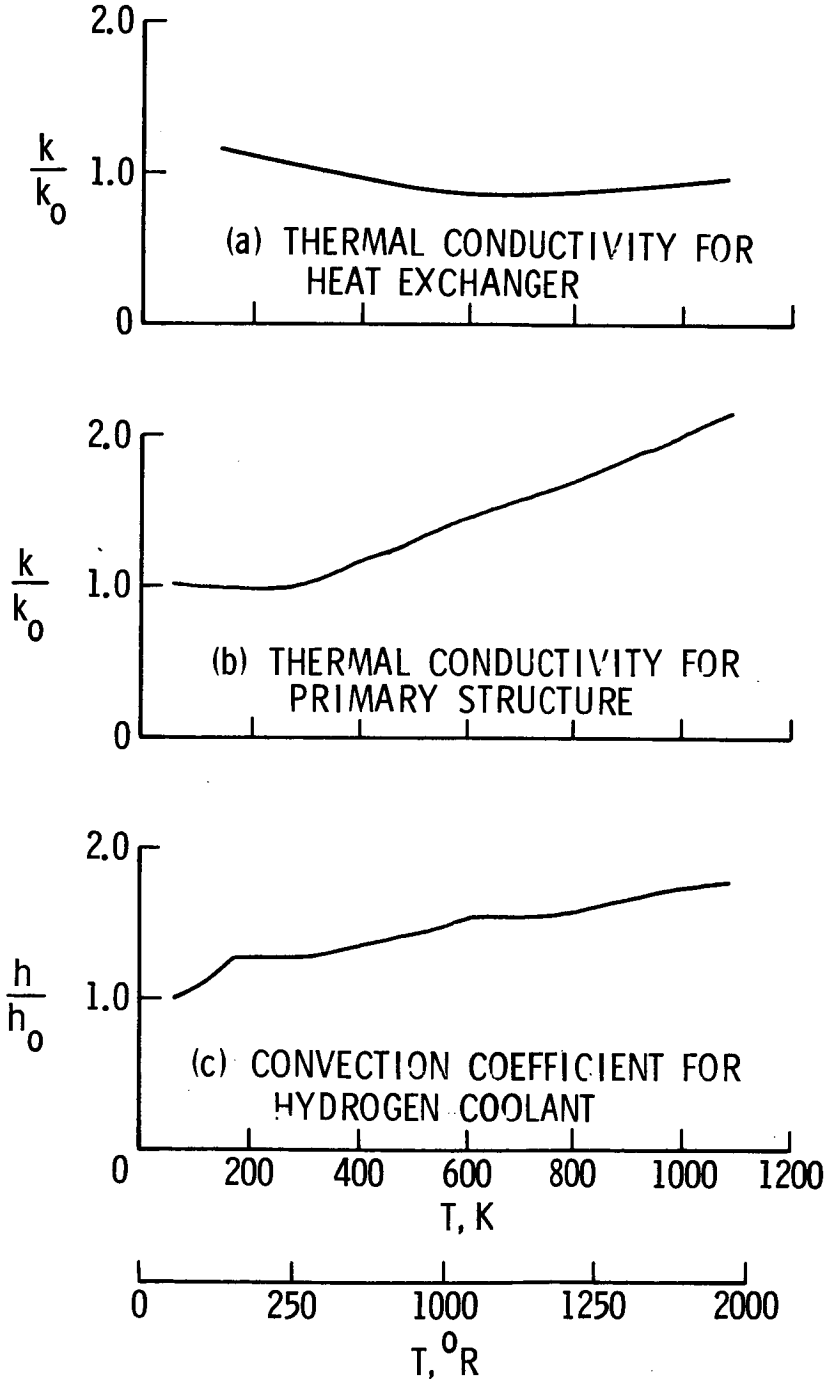

Figure 5. - Variation of heat-transfer coefficients with temperature.

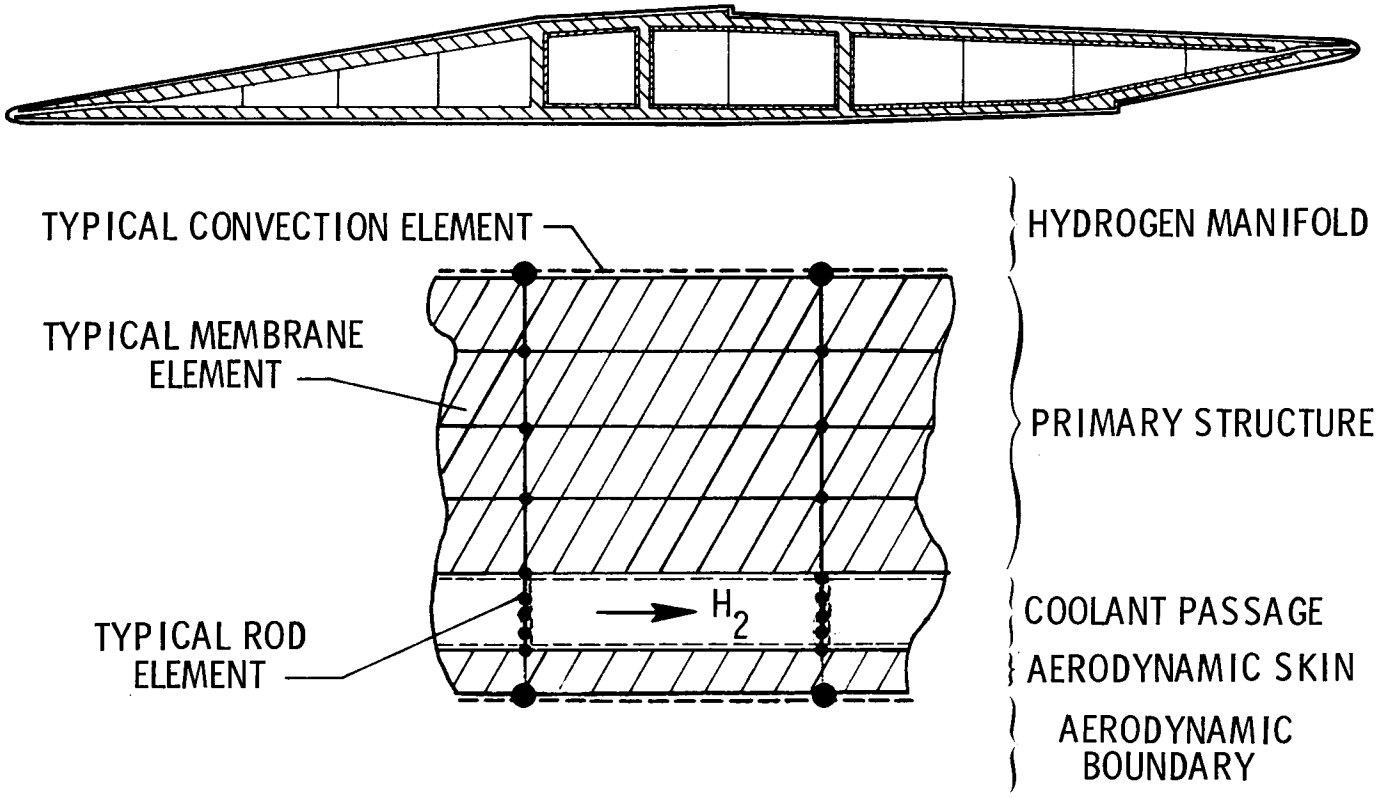

Figure 6. - NASTRAN finite-element model at a typical wall section.

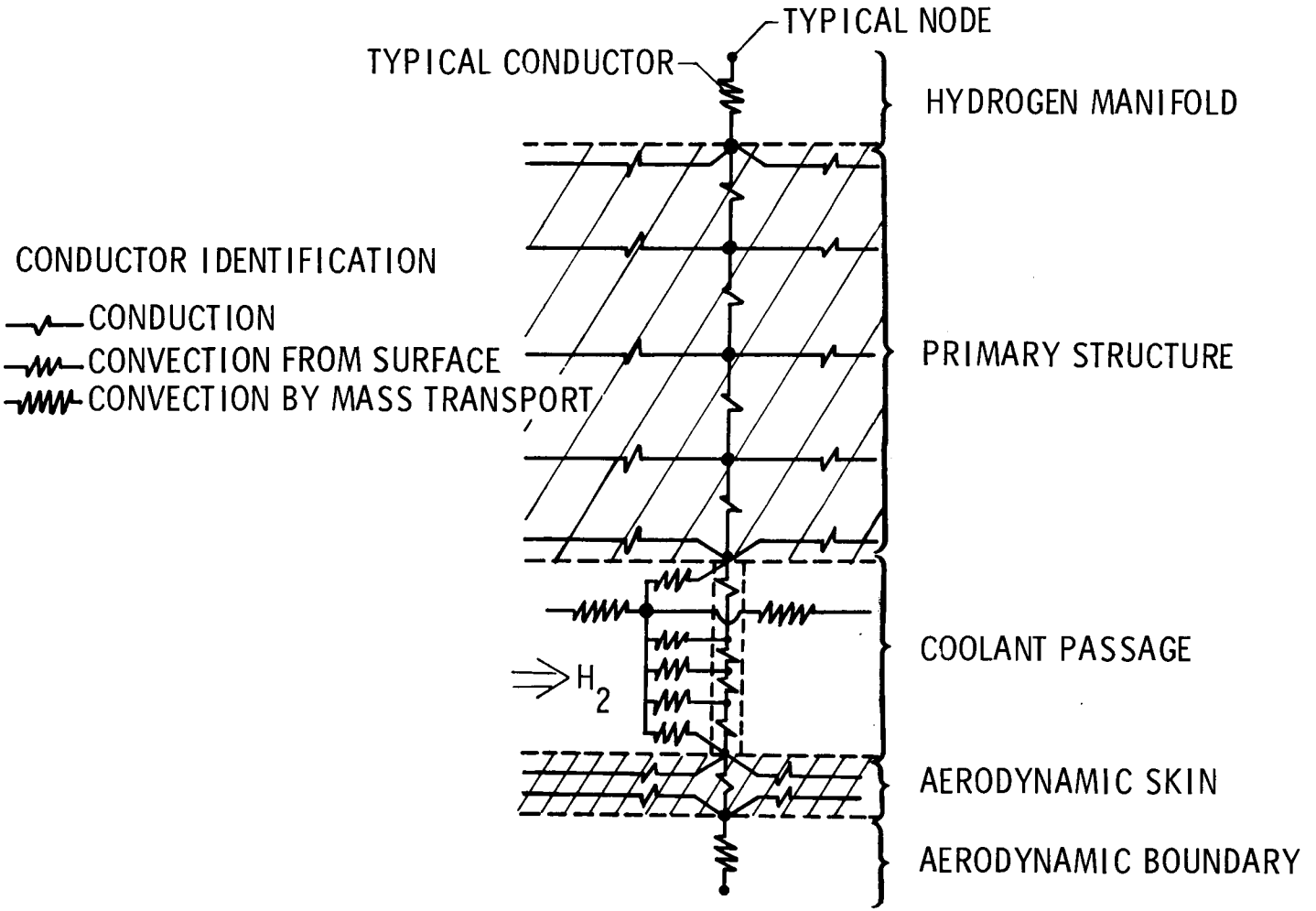

Figure 7. - Typical MITAS thermal model of strut wall section.

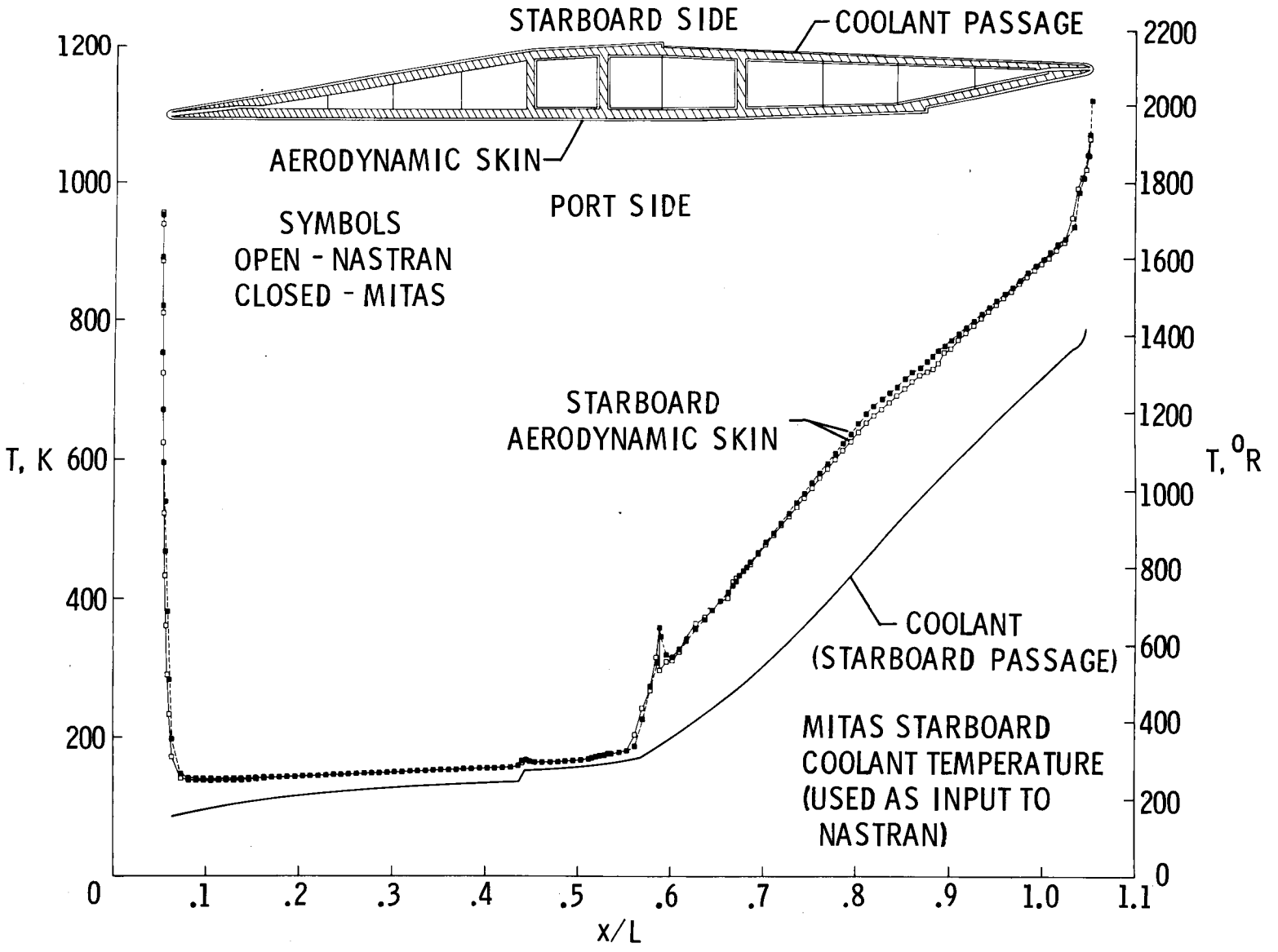

Figure 8. - Comparison of NASTRAN and MITAS predictions for temperature along starboard aerodynamic skin.

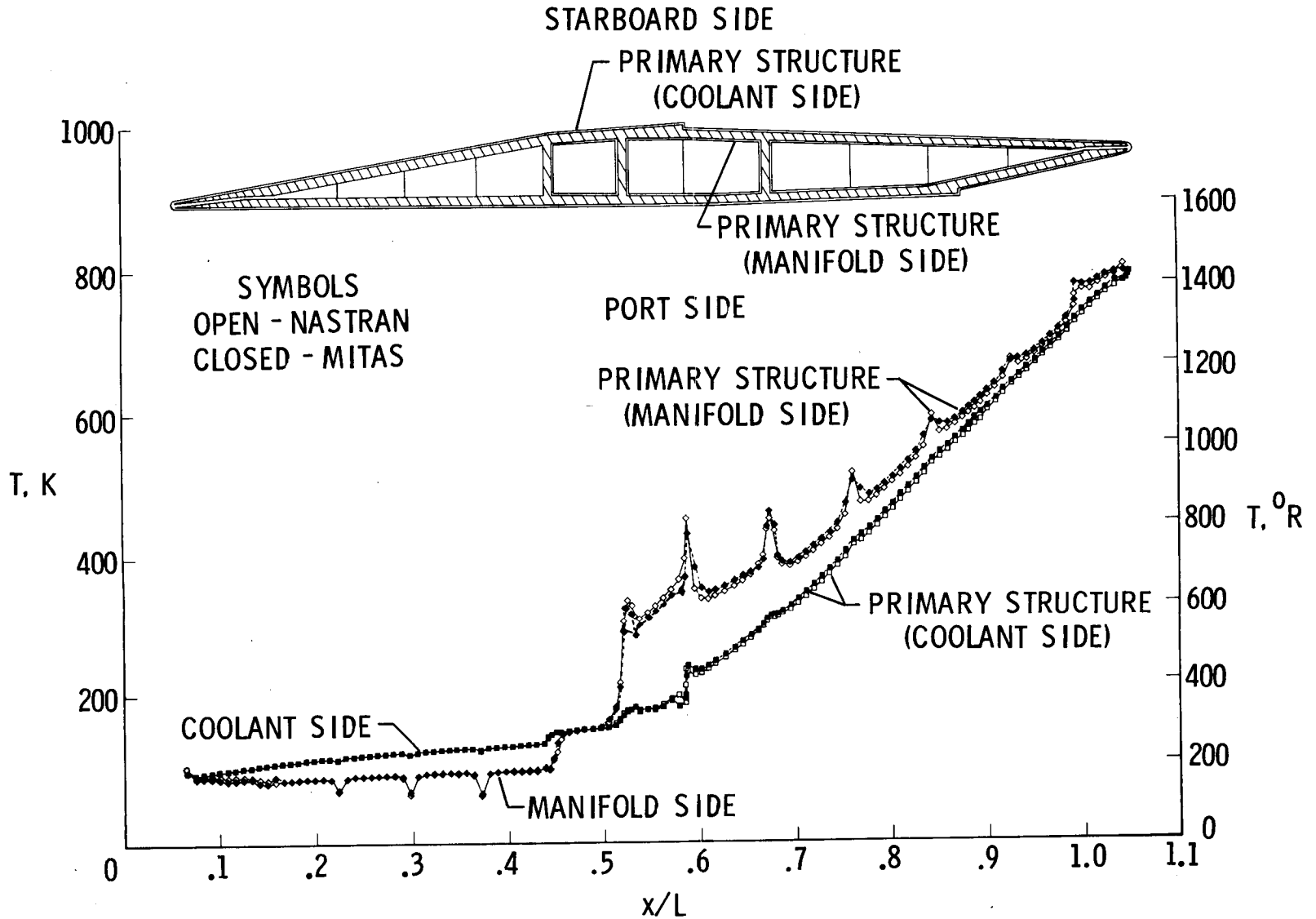

Figure 9. - Comparison of NASTRAN and MITAS predictions for temperature along starboard primary structure.

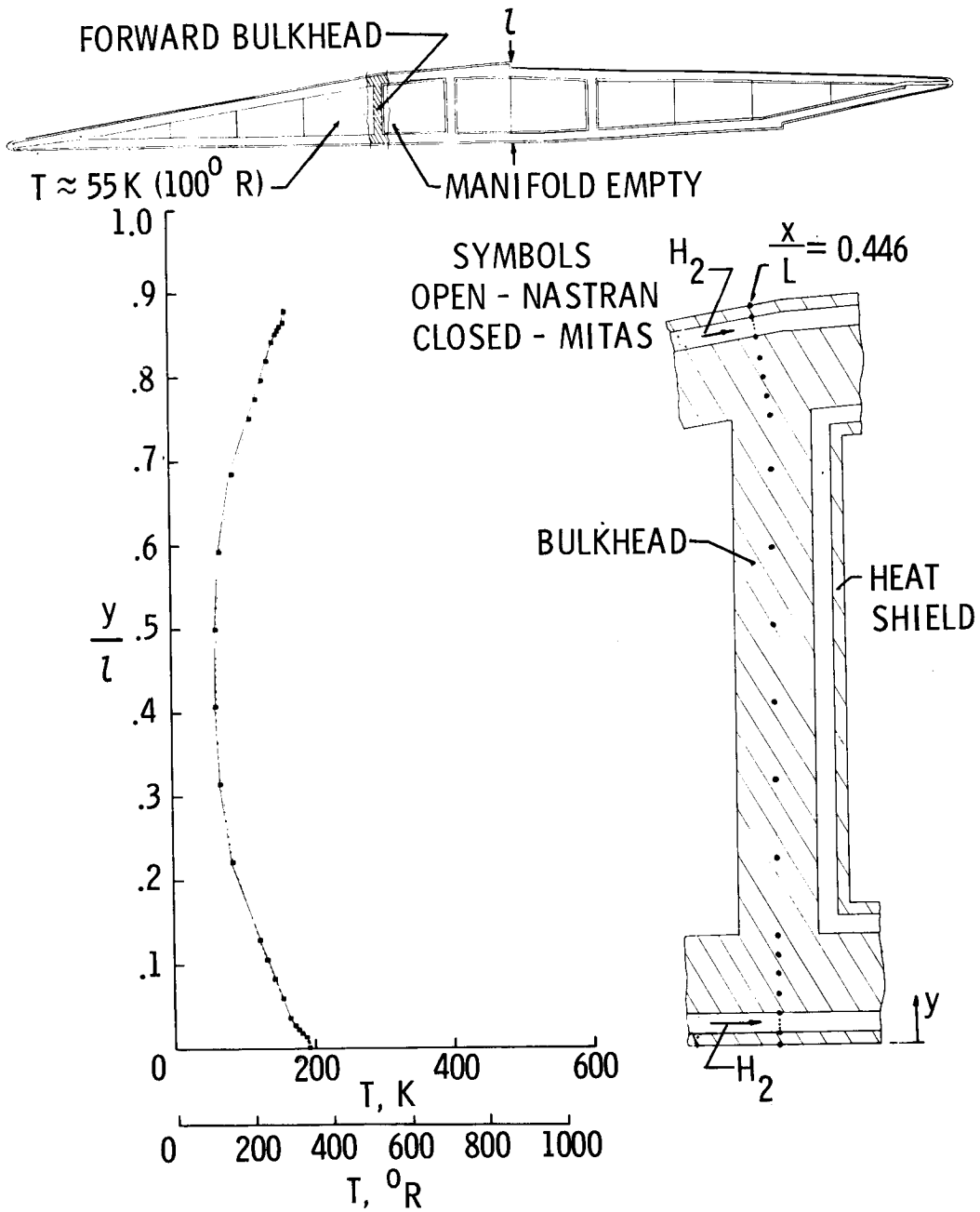

Figure 10. - Comparison of NASTRAN and MITAS predictions for the vertical temperature distribution at the forward bulkhead.

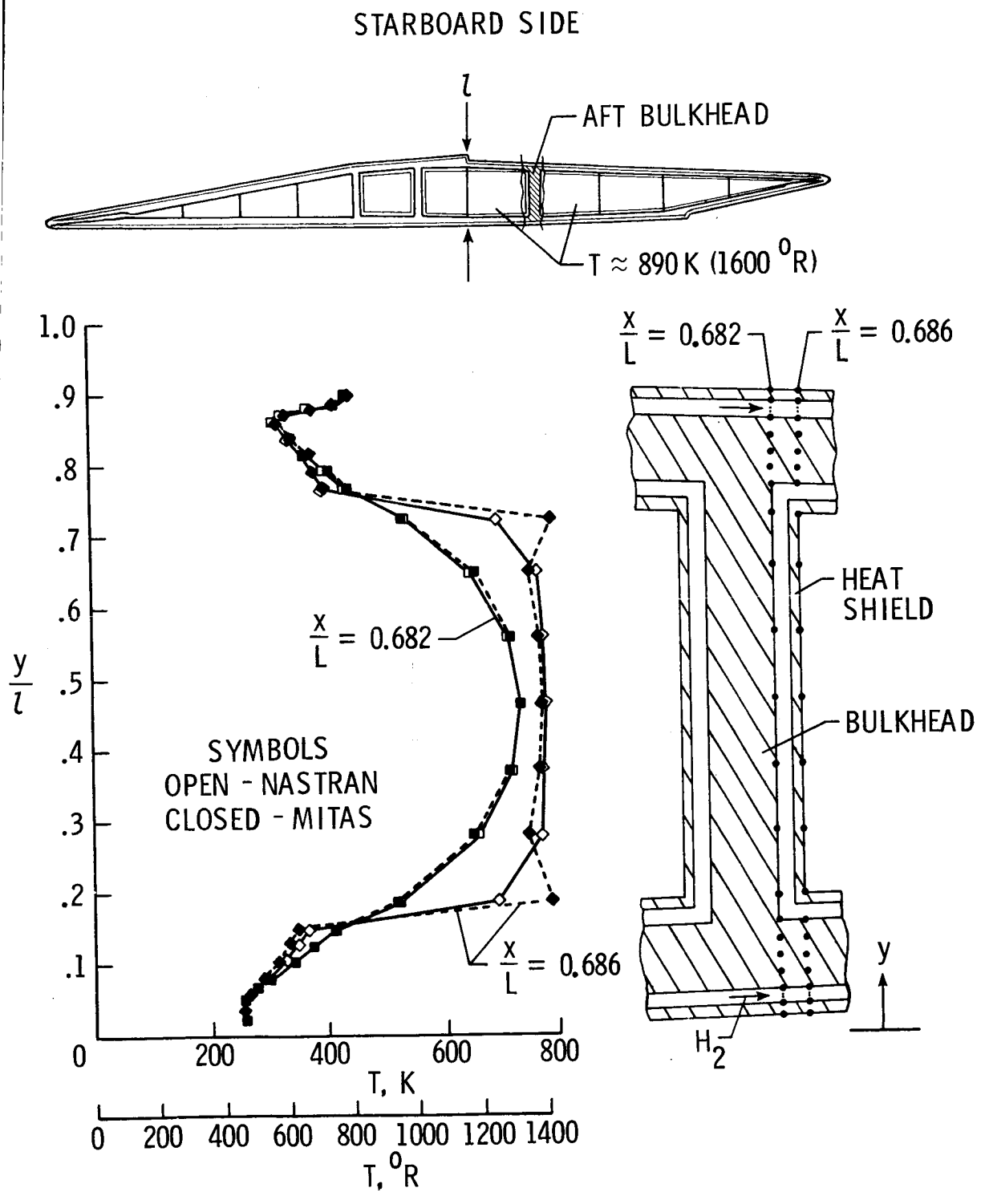

Figure 11. - Comparison of NASTRAN and MITAS predictions for the vertical temperature distributions at the aft bulkhead.